Journal of Power Sources 180 (2008) 742–747

Contents lists available at ScienceDirect

Journal of Power Sources

journal homepage: www.elsevier.com/locate/jpowsour

Short communication

An impedance-based predictive control strategy for the state-of-health of PEM fuel cell stacks

Timo Kurz*, Alex Hakenjos, Jérôme Krämer, Mario Zedda, Carsten Agert

Fraunhofer Institute for Solar Energy Systems ISE, Heidenhofstr. 2, 79110 Freiburg, Germany

ARTICLE INFO

Article history:
Received 14 November 2007
Received in revised form 19 February 2008
Accepted 24 February 2008
Available online 29 February 2008

Keywords:
PEM
Fuel cell
Impedance
Control
Stack
State-of-health

ABSTRACT

This work presents a control strategy for PEM fuel cell systems based on simultaneous impedance measurements on single cells. This control strategy distinguishes between flooding and drying of the cells in a stack and helps to run the stack at an optimal operating point. In the presented experiments, it has been found that impedance measurements can detect flooding phenomena in single cells minutes before they can be seen in related polarisation curves. It is shown that impedance measurements at two specific frequencies, one high and one low frequency impedance, are sufficient to predict voltage drops caused by flooding and drying. In flooding mode, the imaginary part of the low frequency impedance changes while the high frequency impedance remains stable and vice versa in drying mode. This technique reduces measuring time compared to the measurement of whole impedance spectra, without losing important information for the control of the system.

1. Introduction

Polymer electrolyte fuel cells represent a promising technology for portable power applications. Studies predict that portable applications will form the first mass market for commercial fuel cell systems due to the fact that high costs and low lifetime are accepted in favour of high energy densities [1,2]. In contrast to batteries, fuel cell systems need an actively controlled supply of reaction gases. Normally, they also need active heat management [3]. One of the most important problems in PEM fuel cell system control is the complex water management in the stack. In excess water conditions, water vapour in the cells can condense and block the gas transport in the electrodes, gas diffusion layers (GDL) and gas channels. Especially at high current densities, at the cells' maximum power point, it produces a large amount of water which blocks the gas channels. This can lead to unstable cell voltages [4–7]. PEM fuel cell stacks are often operated at a current density below their maximum power point to avoid flooding and to keep the voltages stable. At high voltage and temperature, the cell membranes tend to dry out and their protonic conductivity and mechanical stability decreases [8]. These different failure mechanisms cannot be distinguished in detail by polarisation curves.

Electrochemical Impedance Spectroscopy (EIS) is established as a powerful characterisation tool to detect different failure mechanisms occurring in a fuel cell. Impedance spectra can help to characterise a cell in a much more sophisticated manner than just analysing the polarisation curves. They allow separation between membrane conductivity, kinetic and mass transport limitations [9–12]. Several models exist to examine the current response of fuel cell electrodes and entire fuel cells [13–15]. Fouquet et al. [16] present a fitted impedance model to monitor the state-of-health (flooded, dry and nominal) of PEM stacks.

For the control of a PEM fuel cell system, the cell voltage is commonly used in addition to the stack temperature and the gas fluxes as the main input parameter. As described above, such control strategies often cannot differentiate between drying and flooding of the cell. Furthermore, a voltage drop can only be measured but not predicted, so the control algorithm has to react very rapidly to prevent conditions that lead to power loss or can cause damage to the fuel cell. Thus, model-based control strategies have been developed to acquire more information about the fuel cell conditions so that unfavourable conditions can be prevented and voltages drops can be avoided [17–19].

Mérida et al. [20] show that flooding and dehydration – the two extreme failure modes – can be distinguished by impedance measurements in different frequency bands. They present only impedance measurements of the whole stack and do not detect flooding of single cells. Le Canut et al. [21] present impedance spectra of one cell in a stack during drying and flooding operation.

* Corresponding author. Tel.: +49 76145885205; fax: +49 76145889320.
E-mail address: timo.kurz@ise.fraunhofer.de (T. Kurz).

0378-7753/$ – see front matter © 2008 Elsevier B.V. All rights reserved.
doi:10.1016/j.jpowsour.2008.02.062

Hakenjos et al. [22,23] showed that impedance spectra can detect flooding of single cells in a stack minutes before the cell power decreases. He suggests this measurements to be used in a control strategy.

The present paper develops these approaches one step further by showing impedance measurements on single cells during operation in flooding and drying modes. It also describes how to reduce measuring time by measuring and analysing impedances only at specific frequencies. Finally, a control strategy that uses these measurements to operate a stack by preventing cell flooding and drying is presented and analysed.

2. Experimental

The measurements were carried out using a six-cell stack (described in detail by [24]) with graphite compound bipolar plates. Each cell has an active area of 30 cm^2. Cooling ribs are attached to the two endplates. A controllable fan cools these ribs evenly. The heat of the inner cells is conducted through the stack to reach the cooling ribs. Additionally, this stack contains a humidifying unit located between one of the endplates and the first cell. Thus, an asymmetrical temperature distribution inside the stack is expected. The stack temperature was measured with a Pt-100 resistance temperature device on the surface of the bipolar plate in the middle of the stack.

Large manifolds deliver the feed gases (hydrogen/air) to the single cells to obtain a homogeneous gas supply. On the anode side, hydrogen was fed with a maximum pressure of 200 mbar and recirculated with a pump in a closed loop. This loop can be opened in optional intervals by a purge valve to discharge water and residual gases. In the following, the interval between purge actions is defined as Δt_{purge}, the length of the purge action itself as t_{open}. The open cathode side was supplied with air under realistic humidity and temperature conditions (see Section 3.1). The nominal power output of this stack is 30 W at about 7 A.

For the EIS measurements, a multichannel test bench (described in detail by [22,25]) was used. Temperature and relative humidity of the inlet gases are controllable. Impedance spectra of up to 19 channels can be recorded by using a Solartron 1254 Frequency Response Analyser (FRA) and a Kepco BOP 20-20 M load. To measure the cell impedances, the stack was operated in galvanostatic mode and an ac signal of ±200 mA was impressed on the load current (7 A). This amplitude was chosen to obtain a linear answer of the system (voltage change of $< \pm 10$ mV). The FRA recorded the cell voltages and the ac current signal simultaneously and calculated the resulting impedances.

3. Results and discussion

The following sections describe the procedure from measurement of impedance spectra to stack control design based on impedance values at single frequencies. Firstly, impedance spectra during flooding events are measured. From these spectra, characteristic data are extracted that can predict voltage drops. Secondly, a control concept is presented that uses these values to control a PEM fuel cell stack and prevent voltage drops.

3.1. Impedance spectra during cell flooding

In the standard control approach for the fuel cell system described in [24], single cell voltages in the stack are monitored. In nominal operation, the air stoichiometry is set to a constant level that keeps the stack well humidified ($\lambda = 2.5$, based on empirical data). When one cell voltage drops caused by flooding, the cathode stoichiometry is set to a maximum value limited by the air pump power (λ = approximately 4 . . . 5) until the voltage drop has disappeared.

Table 1
Operating conditions during measurement

Stack temperature (T_{stack})	60 °C
Load current (I)	7 A
Dew point of air (τ_{air})	30 °C
Dew point of hydrogen (τ_{H_2})	−100 °C
Interval between purge time (Δt_{purge})	140 s
Purge time (purge valve open) (t_{open})	3 s
Stoichiometry of air (λ_{air})	2–4
AC amplitude for EIS (ΔI_{EIS})	200 mA
Measurement frequencies (f_{EIS})	75 mHz–1 kHz

The aim of our experiments described below is to operate the stack without this control and to observe what happens before and during these voltage drops. The operating conditions in the following measurements are listed in Table 1. Fig. 1 shows two typical voltage drops occurring in different cells due to cell flooding under the described operating conditions. The air stoichiometry is set to 3. After 233 min, it is decreased to 2 to provoke cell flooding. Immediately, all cell voltages begin to fall slightly, but only cell 6 voltage drops strongly. It reaches a minimum at 241 min. During the following minutes, the voltage rises again, but remains unstable. At 254 min, the air stoichiometry is reset from 2 to 3. After this increase, the voltage rises immediately, indicating that the higher air flux has removed the liquid water from the gas channels and a higher oxygen concentration is available on the catalyst layer.

Cell 5 shows a similar but later and even clearer voltage drop: after 245 min, the voltage begins to decrease significantly. It falls to nearly 0.1 V at 254 min and rises again after the stoichiometry increase, similarly to cell 6.

After the voltage drops, both cell voltages 5 and 6 jump to a higher value than at the beginning, as the cells still profit from their good membrane humidification that reduces protonic conductivity. In comparison, cell 4 shows a nearly constant characteristic during the entire period. This cell in the middle of the stack is not affected by flooding because it is slightly warmer than the outer cells.

In the shown period, impedance spectra of the cells were recorded (measuring 11 points between 75 mHz and 1 kHz). Figs. 2 and 3 display the impedances of cells 5 and 6 at different times during the flooding event (Z0 – Z20). In contrast to Mérida et al. [20], the impedance was measured every 2 min during the whole flooding period.

The impedance spectrum Z0 in Fig. 3(cell 6) still consists of nearly one arc, it represents a well-working cell without mass

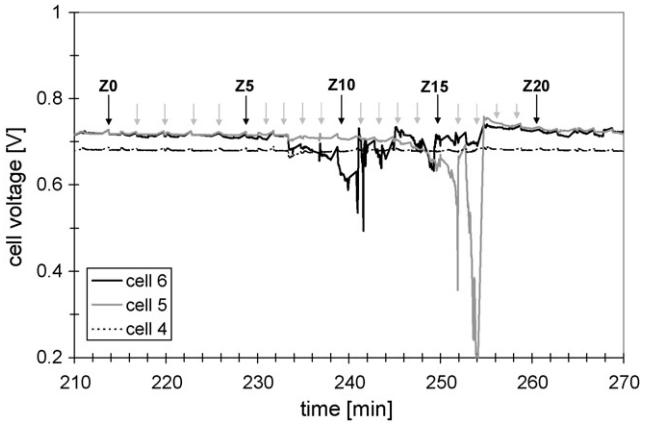

Fig. 1. Cell voltages of three cells during cell flooding events of cells 5 and 6.

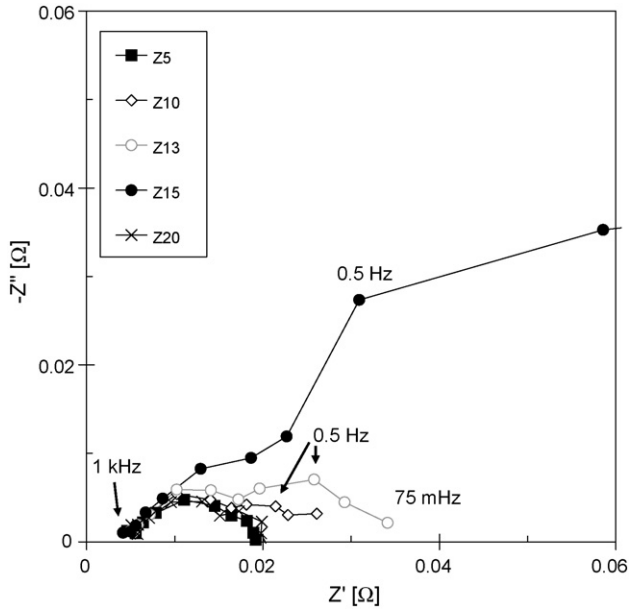

Fig. 2. Impedance spectra of cell 5. The spectra were measured at the times indicated in Fig. 1.

transport problems. The spectra show a strong increase in the low frequency range from Z5 to Z10, after the stoichiometry decrease, indicating mass transport problems in the cell caused by flooding. This low frequency arc increases until Z10. Here, the diameter of this arc is about 0.3 Ω. The spectrum Z15 shows a smaller arc, corresponding to the temporary voltage relaxation at this point. After the increase of air flux, the spectrum Z20 shows a similar characteristic to Z0 before the flooding event. The spectra of cell 5 (Fig. 2) show similar characteristics to cell 6. They begin to expand after Z5, the largest arc can be seen in Z15. After the voltage drop and stoichiometry increase, the arc of Z20 scales down to nearly the size of Z5.

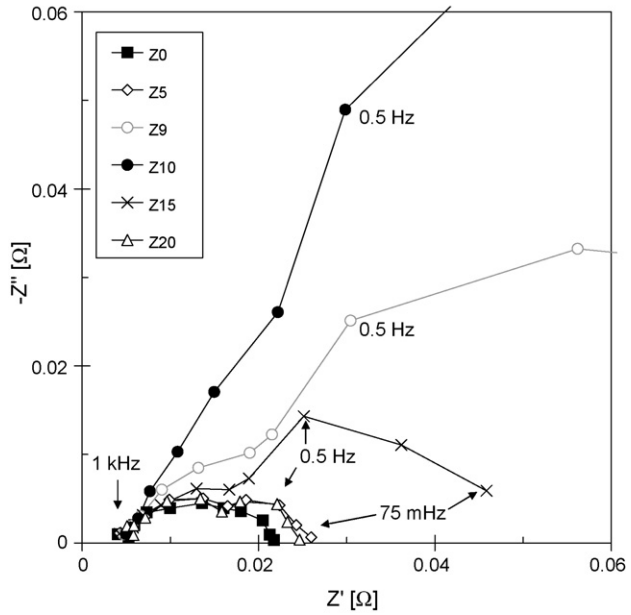

Fig. 3. Impedance spectra of cell 6. The spectra were measured at the times indicated in Fig. 1.

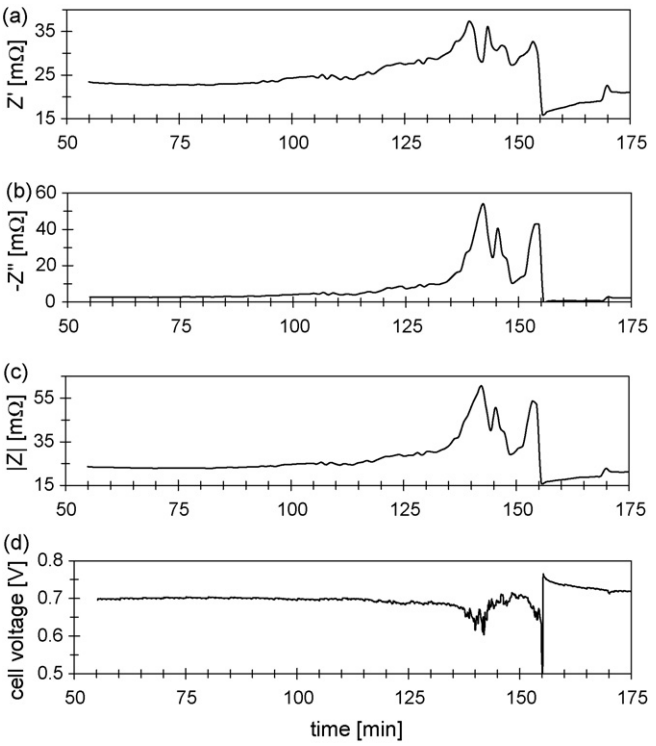

Fig. 4. Impedance of cell 5 at 0.5 Hz: the plots show the real part (a), imaginary part (b), absolute value (c) and the corresponding cell voltage (d).

In the spectra of cells 5 and 6, an increasing low frequency arc appears during cell flooding. The arc starts in all spectra at nearly the same frequency (3.5 Hz, 5th point from right) and enlarges at lower frequencies. While the size and shape of this second arc changes for different spectra, the highest and clearest change can be seen at a frequency of about 0.5 Hz (third point from right). We therefore chose this frequency for the investigation described below.

3.2. Reducing the measuring time

In the measured cell impedance spectra of this stack, an increasing low frequency arc was investigated before and during a cell flooding event. A significant change could be observed at a frequency of about 0.5 Hz. This leads to the conclusion that measuring at only this frequency can save measuring time without losing important information about the humidification state of the cell.

This assumption is confirmed in Fig. 4(a)–(d): they show the change over time of the real part, imaginary part and absolute value of the impedance at 0.5 Hz and the corresponding cell voltage of cell 5 during a flooding event.

The cell voltage begins to decrease slightly the first time after 115 min. It drops strongly at 155 min, falling from nearly 0.7 to 0.5 V, (equivalent to 28%). The other values in the figures above show larger and earlier changes. The greatest change can be seen in the imaginary part (−2.7 to −53.5 mΩ, 2000%). Furthermore, this value is not affected by a shift of the spectrum caused by a higher membrane resistance due to, e.g. drying. For this reason, the imaginary part was chosen as an appropriate parameter for the control concept described in Section 3.4.

In the following, we define the negative imaginary part of the impedance at 0.5 Hz ($-Z''_{0.5\mathrm{Hz}}$) as "Flooding Indication Value" (FIV). For the real part of the impedance at 1 kHz ($Z'_{1\mathrm{kHz}}$), we use the common expression "High frequency resistance" (HFR).

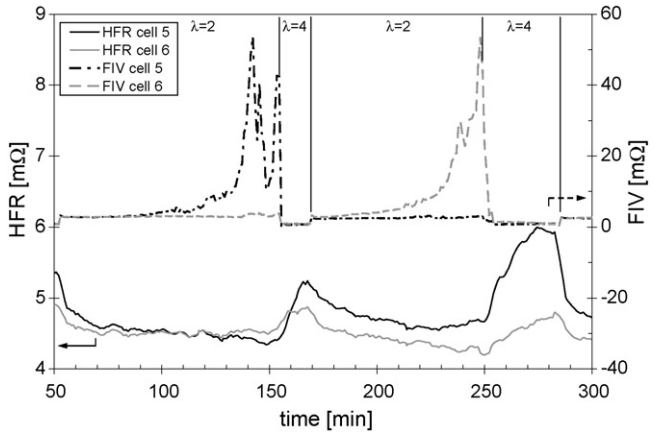

Fig. 5. HFR and FIV of two cells during two flooding events.

3.3. Flooding and drying

Fig. 5 shows the HFR and FIV of cells 5 and 6, now over a longer period than in Fig. 4. The stack was operated at an air stoichiometry of 2. When a voltage drop of cell 5 or 6 appeared, the stoichiometry was set to 4 to purge excess water out of the cell.

The figure shows that both voltage drops of cells 5 and 6 (Fig. 6 at 150 and 250 min) can be early and clearly predicted by looking at the FIV curves: during the first minutes, the impedances as well as the voltages show nearly constant characteristics. After 95 min, the FIV of cell 5 rises from 2.7 mΩ at the beginning to more than 4 mΩ, while the FIV 6 remains constant. The voltage of cell 5 still shows no significant decrease. It begins to fall clearly 20 min later, at 90 min. During the significant voltage drop at around 150 min, the FIV increases to 53 mΩ.

After this voltage drop, the stoichiometry on the cathode side is increased from 2 to 4 for 20 min. After this period, the stoichiometry is reset to 2. Now, FIV 6 begins to increase continuously from 2.7 to 50 mΩ while FIV 5 remains constant. Here, the FIV of cell 6 starts rising nearly half an hour before the voltage of this cell drops significantly.

After the voltage drops of cells 5 and 6, the stoichiometry increase (for 20 and 35 min respectively) leads to a removal of excess water in the cell channels, so the FIV returns to a moderate value and the cell voltage rises. However, during these periods, the HFR begins to rise, indicating that the membrane is drying. The clearest increase from 4.7 to 6.0 mΩ can be seen over a 35-min period for cell 5. A longer drying period would lead to higher HFR values and to decreasing cell performance.

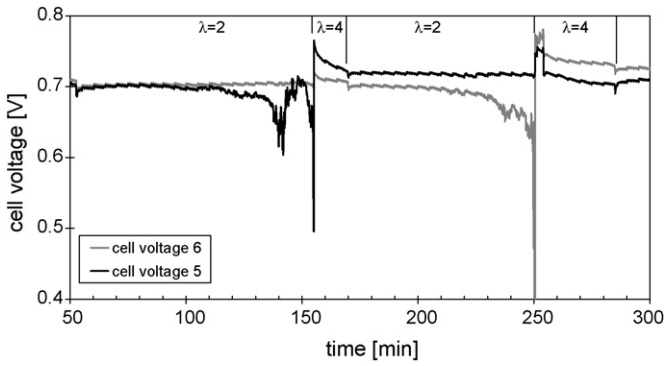

Fig. 6. Cell voltages of two cells during two flooding events.

The plot allows direct comparison of the FIV and HFR values: when the FIV of one cell begins to rise, the HFR remains nearly constant. On the other hand, when the HFR increases, the FIV does not rise, but falls to a slightly lower but constant value.

With these two observations, imminent voltage drops can be predicted reliably and reproducibly by the two values, FIV and HFR. Flooding and drying can be distinguished. Furthermore, measuring only these two values saves time in contrast to measuring whole impedance spectra (as in Figs. 2 and 3).

3.4. Control concept

In the previous section, it was shown that the FIV and HFR are appropriate variables for a real-time control strategy that can predict and therefore prevent voltage drops caused by cell flooding and drying.

Many possibilities exist for the choice of the actuating variable to control the humidification in a fuel cell stack: the stack temperature, the gas temperature and humidification, the purge interval length and the purge time on the anode side, the air flow rate on the cathode side or the load current. The gas temperature and humidification are difficult to adjust and not practical for small systems. In the system used, the purge intervals are set constant and proportional to the load current (every $1000\,\mathrm{s} \cdot I_{\mathrm{load}}$). This interval size is small enough to prevent cell flooding on the anode at the nominal operating point. The system has to supply a constant voltage and power output, so the load current is also not practical as actuating variable. The remaining and most convenient value is therefore the air flow rate: it can be easily adjusted by controlling the air pump voltage and has a direct influence on cell humidity, as seen in Fig. 6. For ideal humidity conditions in a fuel cell stack, every cell should have its own best instantaneous air flow rate [20]. However, in commonly used small fuel cell systems, only the total air flow rate is adjustable. So, in the present paper, the total air mass flow rate was chosen as the control variable.

In Section 3.3, it was shown that the FIV and HFR of a single cell can predict flooding or drying nearly independently of each other: a rising FIV and a constant HFR indicate flooding, a rising HFR and a slightly falling FIV indicate dehumidification under the investigated conditions. This allows us to compress the two values to one, without losing important information.

Thus, the resulting control variable can be expressed as

$$y = \sum_{k=1}^{n} (a \cdot \mathrm{HFR}_k - \mathrm{FIV}_k)\,\mathrm{m\Omega}^{-1}. \quad (1)$$

n is the number of cells in the stack (here: 6). The factor a is an empirical coefficient for the weighting of the two values. It describes the ratio of the change in FIV up to a critical value to the change in HFR to a critical drying value. A value of $a = 2$ gave appropriate control behaviour in our experiments. The resulting control value is used as input variable to a PID control algorithm. The controller then sets the required air flux for the stack as the output variable.

The described control variable is the sum of all cell values and can therefore only react to a change of the overall stack humidity. In the used stack, the outer cells (especially cells 5 and 6, see Section 2) are located nearer to the cooling endplate and are therefore cooler than the inner cells. This leads to an inhomogeneous humidity distribution inside the stack. The outer cells tend to be more humidified than the inner cells. If the FIV of one cell becomes higher and flooding is imminent but at the same time, the HFRs of the other cells are rising, the sum (Eq. (1)) can remain nearly constant and the control cannot intervene. To allow reaction for this scenario, a single cell FIV limit control is additionally implemented:

Table 2
Control parameters

General	
Stack temperature (T_{stack})	50 °C
Relative air humidity (RH_{air})	100%
PID parameters	
Proportional factor (k_p)	0.05
Integration time (T_I)	0.2
Derivation time (T_D)	0 (only PI control)
Other control parameters	
Stoichiometry offset (λ_{offset})	2.9 l/min
Setpoint, $\sum_{k=1}^{n}(2\,HFR_k - FIV_k)$	30.4
Single cell monitoring	
FIV limit (FIV_{limit})	5 mΩ
Stoichiometry increase (air flow pulse) (λ_{pulse})	$\lambda_{actual} + 2$
Duration of air flow pulse (t_{pulse})	30 s

if the FIV of one cell crosses a fixed FIV limit, a short increase of air stoichiometry ($\lambda_{air\,pulse} = \lambda_{actual} + 2$) for 30 s is immediately initiated (in the following called "air flow pulse"). This pulse leads to removal of excess water in the flow channels and the GDL and it is short enough to dry out the cell membranes.

These two control mechanisms together can on the one hand operate the stack in an optimal humidification state and, on the other hand, react to sudden flooding effects in single cells.

3.5. Stack operation with the presented control strategy

The stack was operated with the control strategy described above. Wet conditions were applied (see Table 2) because they represent the most difficult settings for this control strategy by provoking cell flooding. Fig. 7 shows an example of stack operation during a period of 3 h.

The figure clearly demonstrates that controlling has prevented any voltage drops from occuring during the entire period. The periodic small voltage changes (of approximately ±50 mV) are caused by the impedance measurements once per minute.

At varying intervals, an air flow pulse caused by the FIV limit control is initiated, whenever a single cell FIV has crossed the 5 mΩ limit. During the pulse, the cell voltages (and the stack voltage respectively) rise for these 30 s. The resulting stack voltage variation remains below ±2%.

The FIV values of cells 5 and 6 are displayed in Fig. 8 over a shorter period, together with the corresponding control variable and air flow rate. Between 100 and 205 min, the control variable remains below the setpoint (dotted grey line), so the controller increases

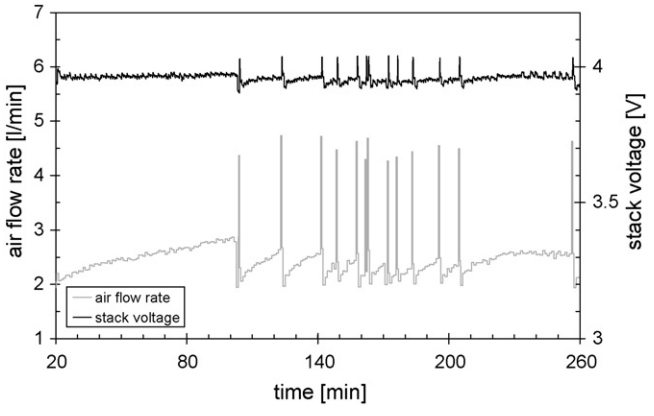

Fig. 7. Stack voltage and air flow rate during 3 h of automatically controlled stack operation under wet conditions. Controlling has prevented voltage drops.

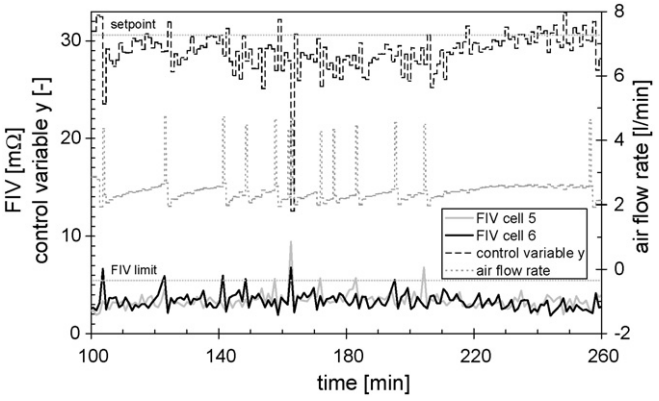

Fig. 8. Control variable y (see Eq. (1)), FIV of cells 5 and 6, and air flow rate during the last 160 min. The FIV limit for the single cell control and the setpoint for the stack control variable are shown with dotted grey lines.

the air flux continuously, trying to raise the control variable. This periods are interrupted by FIV limit overshoots, so an air flow pulse is initiated to avoid flooding. Every FIV limit overshoot is caused either by cell 5 or cell 6. This suggests inhomogeneous cooling of the stack mentioned in Section 2 and therefore an unbalanced humidity distribution in the stack. The FIV overshoots appear during the observed period randomly in cell 5 or 6 and at varying intervals. After every pulse, the controller is reset.

From 205 min onwards, with the same operating conditions, the control variable rises and fluctuates around the setpoint. Here, the PI control alone determines the air flux, without air pulses. It rises continuously to a maximum of around 2.6 l min^2.

These results show that cell flooding events of certain cells under humidified conditions appear stochastically. They are not completly avoidable by a constant moderately high air flow rate. However, the aim in an efficient fuel cell system must be to keep the average flow as low as possible to avoid high parasitic losses, but simultaneously to prevent cell flooding that could cause power drops. This aim is reached by the interaction of the two presented control mechanisms: overall PI control and single cell FIV control. The PI controller sets the air flux in an optimal range and the single cell FIV control prevents imminent flooding events of single cells by initiating short air pulses.

4. Conclusions

In this paper, simultaneous impedance measurements on single cells in a 6-cell PEMFC stack during operation were described. Wet conditions were applied to provoke cell flooding. It was found that impedance spectra can precisely predict cell flooding. Furthermore, two characteristic frequencies were specified that are suitable for use in a control algorithm as input variables to prevent flooding and drying. In contrast to measuring whole impedance spectra, this strategy leads to shorter measurement times and is therefore appropriate for real-time control in small controller platforms. A stack control algorithm was presented that combines the two values, FIV and HFR, to one value without losing information about the humidification state of the stack. This control strategy clearly prevents cell flooding under the described conditions. It consists of two different mechanisms: stack control that regulates the overall stack humidity and single cell control that initiates air pulses to purge excess water out of the gas channels.

The control strategy was demonstrated in stack operation. It operated the stack fully autonomously and was able to prevent all voltage drops caused by flooding.

The presented control algorithm has the potential to be used in other PEMFC systems. It can be adapted to a wide range of operating conditions like stack temperature, current density or gas humidity and stack geometries by adapting its control parameters.

References

[1] C. Hebling, U. Groos, M. Voigt, I. Freesen, European portable fuel cell study: the first expert study on portable fuel cell technologies in europe/a report from: Fraunhofer ISE, Freesen & Partner, VDI/VDE-IT (2003).
[2] World Micro Fuel Cell Markets for Industrial Portable Devices, 2007.
[3] Handbook of Fuel Cells, vol. 4: Fuel Cell Technology and Applications: Part 2, John Wiley & Sons Ltd., 2003.
[4] K. Tüber, D. Pócza, C. Hebling, J. Power Sources 124 (2) (2003) 403–414.
[5] I.A. Schneider, D. Kramer, A. Wokaun, G.G. Scherer, Electrochem. Commun. 7 (12) (2005) 1393–1397.
[6] X. Liu, H. Guo, C. Ma, J. Power Sources 156 (2) (2006) 267–280.
[7] S. Ge, C.Y. Wang, J. Electrochem. Soc. 154 (10) (2007) B998–B1005.
[8] T. Springer, T. Zawodzinski, S. Gottesfeld, J. Electrochem. Soc. 138 (8) (1991) 2334–2341.
[9] P. Kurzweil, H.J. Fischle, J. Power Sources 127 (1–2) (2004) 331–340 (Selected Papers from the Ninth Ulm Electrochemical Days).
[10] T. Springer, I. Raistrick, J. Electrochem. Soc. 136 (6) (1989) 1594–1603.
[11] I. Raistrick, Electrochem. Acta 35 (10) (1990) 1579–1586.
[12] T.J.P. Freire, E.R. Gonzalez, J. Electroanal. Chem. 503 (1–2) (2001) 57–68.
[13] T. Springer, T. Zawodzinski, M. Wilson, S. Gottesfeld, J. Electrochem. Soc. 143 (2) (1996) 587–599.
[14] V. Paganin, C. Oliveira, E. Ticianelli, T. Springer, E. Gonzales, Electrochim. Acta 43 (24) (1998) 3761–3766.
[15] D. Gerteisen, A. Hakenjos, J.O. Schumacher, J. Power Sources 173 (1) (2007) 346–356.
[16] N. Fouquet, C. Doulet, C. Nouillant, G. Dauphin-Tanguy, B. Ould-Bouamama, J. Power Sources 159 (2) (2006) 905–913.
[17] J. Golbert, D.R. Lewin, J. Power Sources 135 (1–2) (2004) 135–151.
[18] J.H. Lee, T.R. Lalk, J. Power Sources 73 (2) (1998) 229–241.
[19] J.C. Amphlett, R.F. Mann, B.A. Peppley, P.R. Roberge, A. Rodrigues, J. Power Sources 61 (1–2) (1996) 183–188.
[20] W. Merida, D. Harrington, J. Le Canut, G. McLean, J. Power Sources 161 (1) (2006) 264–274.
[21] J.M. Le Canut, R.M. Abouatallah, D.A. Harrington, J. Electrochem. Soc. 153 (5) (2006) A857–A864.
[22] A. Hakenjos, M. Zobel, J. Clausnitzer, C. Hebling, J. Power Sources 154 (2) (2006) 360–363 (Selected Papers from the Ninth Ulm Electrochemical Days).
[23] A. Hakenjos, Untersuchung zum Wasserhaushalt von PEM-Brennstoffzellen, Dissertation, Albert-Ludwigs-Universität (2006).
[24] M. Oszcipok, M. Zedda, J. Hesselmann, M. Huppmann, M. Wodrich, M. Junghardt, C. Hebling, Portable proton exchange membrane fuel-cell systems for outdoor applications, J. Power Sources 157 (2).
[25] A. Hakenjos, C. Hebling, J. Power Sources 145 (2) (2005) 307–311 (Selected Papers Presented at the Fuel Cells Science and Technology Meeting).